K. Li, Z. Ma, X. Huang, Y. Zou (2022) *Merging Dynamics of Dual Parallel Linear Diffusion Flames*, **Fire Safety Journal,** 127, 103490. https://doi.org/10.1016/j.firesaf.2021.103490

Merging Dynamics of Dual Parallel Linear Diffusion Flames

Kaiyuan Li[1,*], Zhuangzhuang Ma[1], Xinyan Huang[2,*], Yanyan Zou[1]

[1]*School of Safety Science and Emergency Management, Wuhan University of Technology, China*

[2]*Research Centre for Fire Safety Engineering, Department of Building Environment and Energy Engineering, The Hong Kong Polytechnic University, Hong Kong SAR*

* Corresponding to kyli@whut.edu.cn (K. Li), xy.huang@polyu.edu.hk (X. Huang)

Abstract:

The merging of flames is a widely observed fire phenomenon in building and wildland fires. This work explores the merging characteristics of two identical linear diffusion flames. The duel parallel linear burners are used (dimensions of 100 mm×4 mm and 200 mm×2 mm), and the heat release rate (HRR) of each buoyancy-driven flame varies from 0.7 to 10.9 kW. The flame merging probability and merging flame height are quantified under different spacing of burners and HRRs. A new dimensionless HRR involving the aspect ratio is proposed to determine the merging probability. Moreover, decreasing the entrained air from the ground promotes the flame merging, which can be reflected by an increase of dimensionless HRR. The merging flame height is determined by the competition of buoyancy and pressure difference around the flame, which can be correlated by the effective entrainment perimeter and the dimensionless HRR. Such a correlation can also be used to explain the flame merging phenomena with different HRRs and aspect ratios in the literature.

Keywords*: flame merging; merging probability; merging flame height; aspect ratio; entraining air.*

Nomenclature

A	characteristic length (m)	$\dot{Q}^*$	dimensionless HRR
c_p	specific heat capacity (kJ/(kg · K))	R	air entrainment perimeter (m)
D	constant	S	burner spacing (cm)
d	characteristic length (m)	S_t	air to fuel mass stoichiometric ratio
d_s	equivalent diameter of the burner (m)	T	temperature (K)
D	characteristic length of burner (cm)	$\overline{\Delta T_f}$	average flame temperature rise (K)
Fr	flame Froude number	u_f	fuel velocity at the burner outlet (m/s)
Re	Reynolds number	W	width of burner (mm)
g	gravitational acceleration (m/s^2)		
ΔH_c	heat of combustion (MJ/kg)	*Greeks*	
K	the characteristic length (m)	α	coefficient
L	length of burner (mm)	ρ_∞	ambient air density (kg/m^3)
L_c	characteristic length (m)		
L_{c1}	dimension variable (m)	Subscripts	
n	burner aspect ratio	∞	ambient
N	number of frames with merging flame	0	no mergin
Nb	the number of burners	n	aspect ratio
Pm	merging probability	p	air entrainment
$\dot{Q}$	heat release rate (HRR)	R	air entrainment perimeter

1 Introduction

The burning and spreading of multiple fires simultaneously is a common phenomenon in building and wildland fires. In addition to the large-scale and multiple strong fires such as the crown fires [1], multiple vehicles burning in tunnel fires [2-4], and multiple fires caused by fuel leakage [5, 6], there are also linear flames with relatively small scales and low heat release rates (HRRs), such as flames from char fissures and cable flames shown in Fig. 1. At present, there is little knowledge about the merging characteristics of such linear flames, which are usually driven by buoyancy but have restricted air entrainment.When two flames are close to each other, the flame will be tilted due to the restriction of air entrainment, and eventually, merge under certain conditions with an increased flame height [7]. The air entrainment behaviours of linear burners with high aspect ratios differs from those of square and circular burners. The linear flames with low HRR are likely to be more sensitive to the environment and the flame merging behaviors are more complex. Besides, investigating the merging flames leads to the foundations of reproducing the flame structures on the surface of burning materials, for predicting the heat flux field in the future. To better understand the combustion and merging behaviors of linear flames with low HRR and high aspect ratios, it is worthwhile carrying out corresponding investigations.

(a) Separate fissure flames (b) Merging cable flames

Fig. 1. Multiple flames with low heat release rates and high aspect ratios, (a) separate fissure flames and (b) merging cable flames.

For the merging flames [8], the previous researches mainly focused on the merging probability [3, 9-13], and the height [3, 9-12, 14-19], temperature [20] and velocity distributions [21], and heat fluxes [22]. Particularly, the merging probability and merging flame height have been mostly studied, as summarized in Table A1 of the Appendix. The merging probability of dual flames is usually correlated with the burner spacing *S*, the stand-alone flame height $L_{f,0}$, the merged flame height of zero burner spacing, $L_{f,S=0}$, the HRR $\dot{Q}$, burner length *L* (*D* for square shape) and width *W*. For example, Hu et al. [9] conducted a set of experiments with a burner size of 142.5 mm×2 mm and proposed a correlation of merging probability and dimensionless burner spacing, $\frac{S}{L_{f,0}}$. Wan et al. [10] experimentally studied the merging behaviors of two square gas flames, where a critical condition of flame merging was found as $\frac{S}{L_{f,S=0}} = 0.3$. Tao et al. [11] conducted a set of flame merging experiments using the burners with different dimensions and proposed a correlation predicting the merging probability using a dimensionless HRR involving $\dot{Q}$, *S*, *L* and *W*. However, the aspect ratio in Tao's experiments was only up to 8, which did not fall into the "linear flame" category, so the model may not be suitable for high aspect ratios. Liu et al. [12] proposed a characteristic length of $Z_c = \left(\frac{\dot{Q}}{\rho_\infty c_p T_\infty L\sqrt{g}}\right)^{\frac{2}{3}}$ and established a correlation of merging probability and $\frac{S}{z_c}$ for the flames with different burner lengths. These previous studies suggest that the dimensionless burner spacing controls the merging probability, while the existing models has not yet covered the effects of low heat release rate and high aspect ratio.

Compared to the merging probability, the merging flame height is a more intuitive presentation of flame merging. In previous studies, it is found that the merging flame height is mainly affected by $\dot{Q}$, *S*, $L_{f,S=0}$, *D*, *L*, and *W* [23]. Hu et al. [9] studied the merging behaviors of two linear diffusion flames. The merging flame height was predicted with a modified entrainment perimeter, $P = L + 2W + S + \alpha L$, as the characteristic length. Wan et al. [10] carried out a series of experiments on two square burners

and conducted a theoretical analysis on the air entrainment mechanism to propose the mathematical models for the merging flame heights in open space and under tunnel ceiling. The merging flame heights were found strongly related to *D* and *S*. Tao et al. [11] took into account the influences of burner dimensions and proposed a model for predicting the merging flame height. However, in the model the merging flame height was determined only by *L* and *W* while the effects of *S* were not included, therefore, the model was not suitable for the intermittent flame merging and non-merging cases. Liu et al. [12] proposed a correlation of dimensionless merging flame height and HRR using the concept of "merging state", which indicated that the merging flame height was mainly determined by *L*, *W* and *S*. Sugawa and Takahashi [14] carried out an experimental study on dual rectangular flames, the merging flame of zero burner spacing was regarded as a single fire and $L_{f,S=0}$ was used as the characteristic length to develop a correlation of merging flame height and burner dimension and spacing. Kamikawa et al. [15] and Delichatsios [16] studied the square burner array. Wang et al. [17] and Liu et al. [18] studied the dual jet fires. The details were also summarized in Table A1 of the Appendix. He et al. [19] carried out a study on two rectangular flames with different aspect ratios and proposed a merging flame height model with $\frac{2LS}{L+S}$ as the characteristic length. However, the aspect ratio was only up to 8, hence, the feasibility of the model on high aspect ratio was challenged. So far, few experiments are available to study the linear diffusion flames with low HRRs and high aspect ratios.

This study focuses on the merging characteristics of two linear flames with relatively low HRRs and high aspect ratios. The probability and height of flame merging are investigated experimentally. Then, the merging probability and merging flame height under different merging states are explored theoretically with the dimensionless analysis.

2 Experiments

2.1 Experimental setup

Figure 2 shows the experimental facility, where two identical burners are used with the outlets flushed at the same horizontal plane. The burners are made of stainless steel with a thickness of 2 mm. Each burner is composed of a rectifier and a rectangular nozzle. The rectifier is filled with quartz particles of uniform size to ensure a uniform outlet flow rate. In the current study, two linear-burner dimensions are used, (1) 100 (*L*) mm×4 (*W*) mm and (2) 200 mm×2 mm, so that they have the same area but different aspect ratios (*L/W*) of 25 and 100, respectively (see Table 1). Propane is used as the fuel, and its effective heat of combustion (ΔH_c) is about 46.3 MJ/kg [24]. The HRRs of both burners are kept the same and controlled by a flow meter, while the range of total fuel flow rate is 1-15 L/min. For each burner, the range of HRR is 0.7-10.9 kW, leading to the outlet velocity of 0.042-0.630 m/s. The range of burner spacing, *S*, is 0-20 cm, which is measured from the long sides of the burners (see Fig. 2).

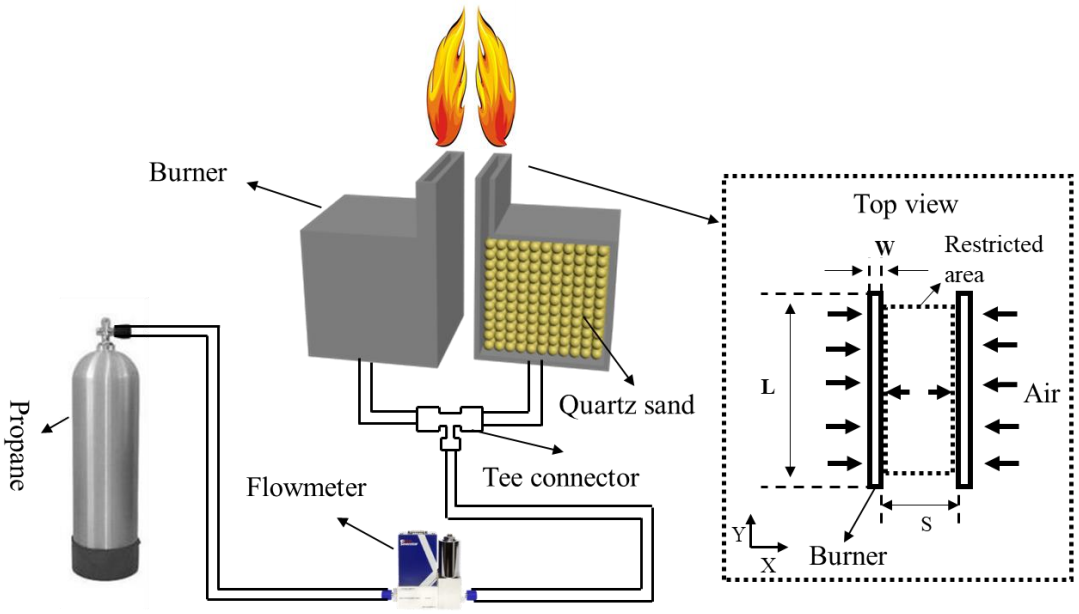

Fig. 2. Experimental setup

The experiment process was recorded using a Sony FDR-AX60 camera with a frame rate of 25 FPS. The resolution is 3840×2160 pixels, and the camera was placed 1.3 m away from the burner. The laboratory is 6 m long, 3 m wide, and 4 m high, which ensures sufficient air supply during the experiment. Once each experiment was finished, the ventilation was set off to exhaust the smoke for the next experiment. The ambient temperature is approximately 13 ℃. The experimental conditions are summarized in Table 1. Each experiment was repeated twice to ensure the repeatability.

Table 1. Experimental conditions and burner specifications.

Burner size (mm)	Burner spacing, S (mm)	Total fuel flow rate, $\dot{Q}_F$ (L/min)	Outlet velocity, u_F (m/s)	HRR of each burner (kW)	Re (-)	Fr number (-)
100×4	0, 10, 20, 30, 40, 50, 60, 80, 100, 150, 200	1, 2, 3, 4, 5, 6	0.042, 0.084, 0.126, 0.168, 0.210, 0.252	0.73, 1.45, 2.18, 2.91, 3.63, 4.36	269.58-1010.91	0.00155-0.00931
200×2	0, 10, 20, 30, 40, 50, 60, 80, 100, 150, 200	4, 5, 6, 8, 10, 12, 15	0.168, 0.210, 0.252, 0.294, 0.336, 0.378, 0.420, 0.504, 0.630	2.91, 3.63, 4.36, 5.81, 7.26, 8.72, 10.89	33.69-202.18	0.00878-0.0329

2.2 Image processing

The videos are processed using the OpenCV image processing library in python [25]. Figure 3 presents the flame image processing procedure [26-28]. Firstly, for each test condition, a 60-s flame video of steady-state is extracted and converted into 1,500 flame pictures (frames). Then, the flame pictures are converted into grayscale followed by the binary version with Otsu's method [18]. Afterward, the probability of each pixel is averaged for the 1,500 binary pictures to obtain the probability profile.

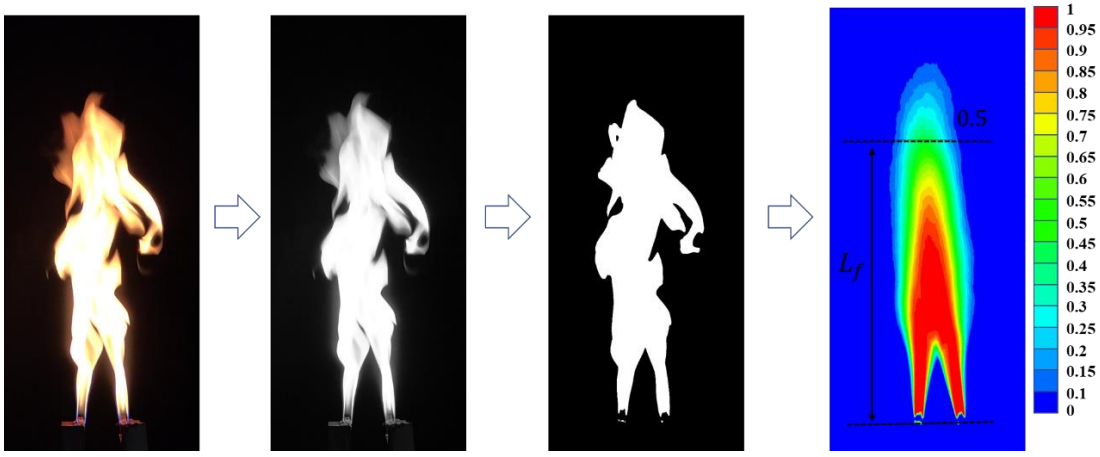

(a) Flame picture (b) Grayscale (c) Binary (d) Probability profile

Fig. 3. Image processing procedure

3 Results and Discussions

3.1 Combustion and flame merging states

Delichatsios [29] introduced the flame Froude number, Fr_f, as a parameter to illustrate whether the flame is controlled by the buoyancy flow (Fr < 1) or the momentum flow (Fr >1)

$$Fr_f = \frac{u_f}{(gd_s)^{\frac{1}{2}}(S_t+1)^{\frac{3}{2}}(\rho/\rho_\infty)^{\frac{1}{4}}(\overline{\Delta T_f}/T_\infty)^{\frac{1}{2}}} \quad (1)$$

where u_f is the fuel velocity at the burner outlet, d_s is the equivalent diameter of the burner, which is replaced the hydraulic diameter for linear flame, S_t is air to fuel mass stoichiometric ratio which is 15.8 for propane, ρ is the fuel density of 1.83 kg/m^3 of propane, $\overline{\Delta T_f}$ is the average flame temperature rise of 900 K [9]. The calculation results show that Fr_f ranges of 0.00155-0.0329 for all experiments, as presented in Table 1. The maximum value is far low than the 1 threshold for the momentum controlled flames [29], thus, the influence of fuel velocity on the flame can be ignored. Hence, all flames in the current paper can be regarded as buoyancy-driven diffusion flames. Meanwhile, Table 1 shows that the range of *Re* number in all experiments is 33.69-1010.91 (*Re*<2000), indicating that the initial fuel flows are laminar [30].

Figure 4 shows the typical merging behaviors under different HRRs and burner spacings. It can be seen that with increasing *S* the flame merging presents three different behaviors (or Regimes), i.e. (I) the completely merging, (II) the intermittently merging, and (III) no merging [10]. When *S* is relatively small, the dual flames merge completely. As *S* increases, there is a transition of flames from completely merging to intermittently merging. When *S* is large enough, the two flames burn freely without affecting each other. At the stage, the dual flames are basically the same as two single independent flames. Under the same *S*, as the HRR and aspect ratio of the burner increase, the flames become easier to merge. As shown in Fig. 4, generally, as burner spacing (S) increases, the merging flame height decreases.

However, unlike the previous momentum-controlled jet flames [13], the merging flame height presents a non-monotonic trend in the current set of experiments (described in detail in the later section).

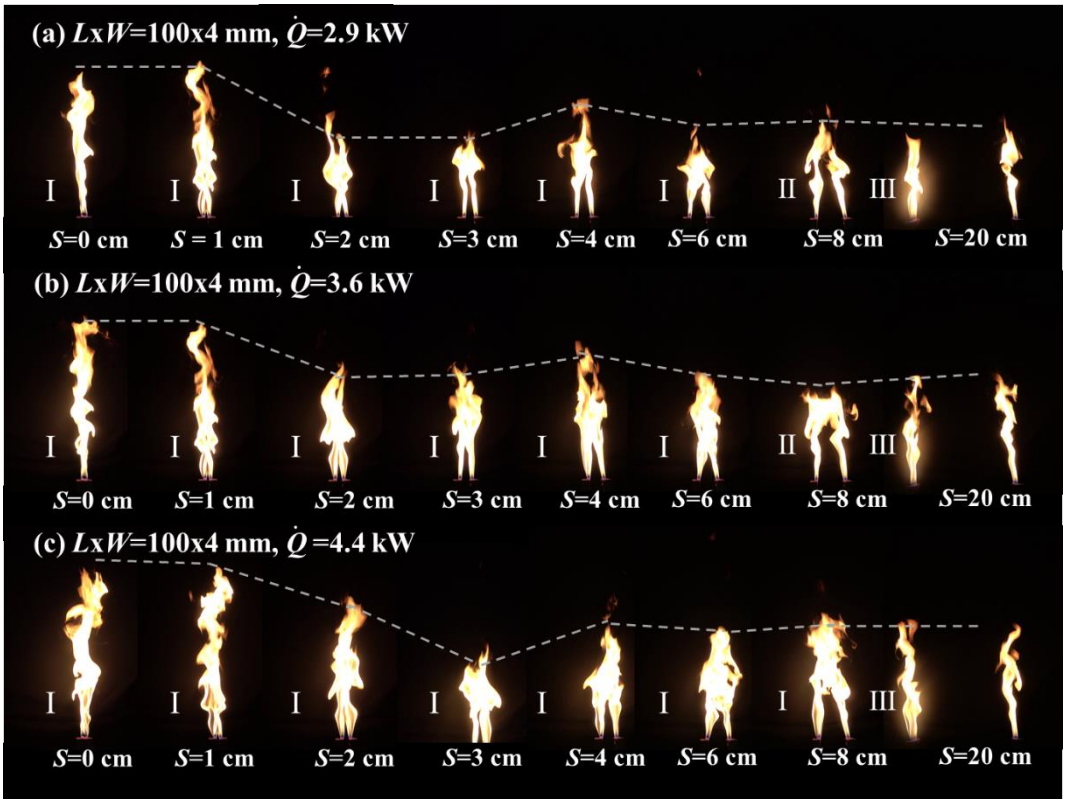

(a) 100×4 mm burner

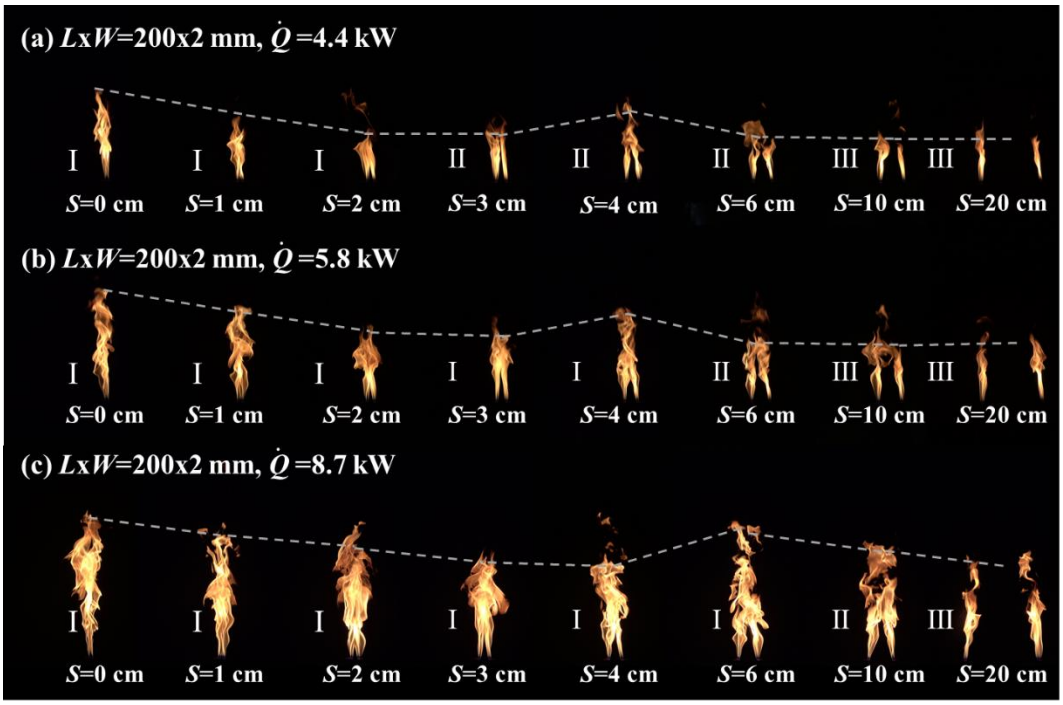

(b) 200×2 mm burner

Fig. 4. Flame merging behaviors under different HRRs and burner spacings

3.2 Merging probability

The presence of flame on the centerline of the two burners is used to determine flame merging [12], and in each experiment, the number of frames with flame merging is divided by the total number of frames to calculate the merging probability as [28]

$$P_m = \frac{N}{N_{total}} \tag{2}$$

where P_m is the merging probability, N is the number of frames with merging flame, and N_{total} is the total number of sampling frames.

Figure 5 shows the flame merging probability under different HRRs and burner spacings. For intermittently merging (regime II), the merging probability increases with increasing HRR under the same burner spacing (S) as

$$P_m \propto \dot{Q} \tag{3}$$

where $\dot{Q}$ is the HRR of a single burner. Moreover, under the same HRR, the merging probability increases with the decreasing S. Previous study on dual diffusion flames [28, 31] suggested that the merging probability has a functional relationship with the dimensionless burner spacing ($\frac{S}{L_{f,0}}$)

$$P_m \propto -\frac{S}{L_{f,0}} \tag{4}$$

where $L_{f,0}$ denotes the flame height when no merging takes place (single flame). Hu et al. [9] investigated the flame merging probability with an aspect ratio of 71.25 and found that P_m and $\frac{S}{L_{f,0}}$ can be linearly correlated as

$$P_m = -3.63\frac{S}{L_{f,0}} + 2.31 \tag{5}$$

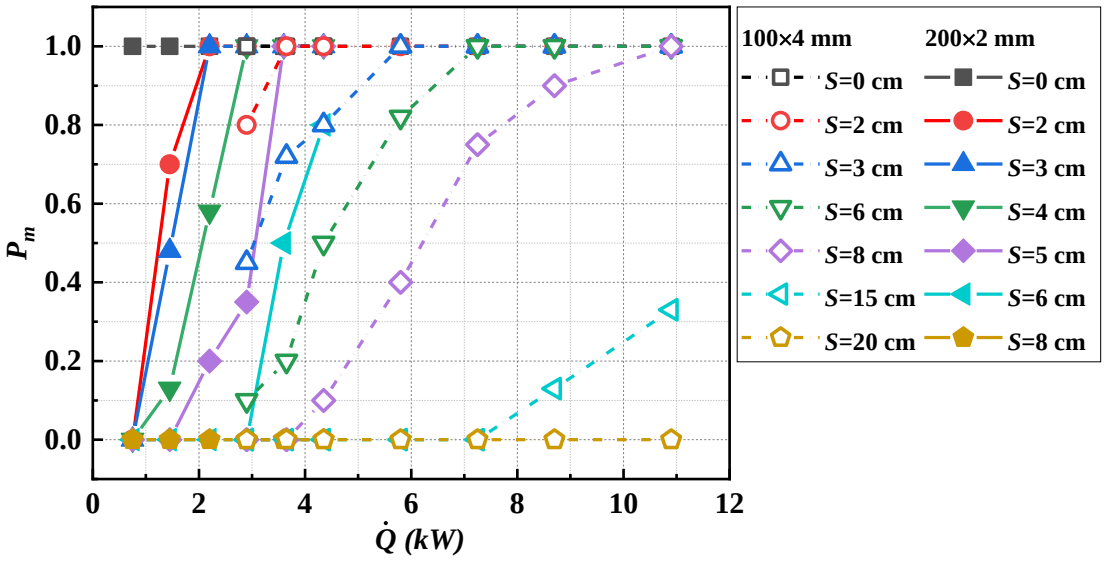

Fig. 5. Merging probability under different HRRs and burner spacings

Figure 6 plots the P_m against $\frac{S}{L_{f,0}}$ under several aspect ratios, including the data in the current study and literature [9-12]. From Fig. 6, P_m and $\frac{S}{L_{f,0}}$ have a negative linear correlation, and with only $\frac{S}{L_{f,0}}$ a generalized predictive model can not be developed for all aspect ratios. Note that the aspect ratio, *n*, denoting the degree of linearization, has a notable impact on the merging probability. According to the previous analysis, the flame merging is mainly caused by the internal and external pressure difference between the two flames [10]. When *n* increases, the restricted entrainment perimeter increases, which makes it easier to form pressure differences, leading to flame merging. This trend can be seen in Fig. 6, where P_m increases with *n*. Therefore, P_m and *n* can be correlated as

$$P_m \propto n = \frac{L}{W} \tag{6}$$

Combining Eqs. (3), (4), and (6), it can be inferred that the HRR and flame height of a single burner, burner spacings, aspect ratio, length and width of the burner should be the key parameters that control the merging probability as

$$P_m = f(\dot{Q},\ L_{f,0},\ S,\ n,\ L,\ W) \tag{7}$$

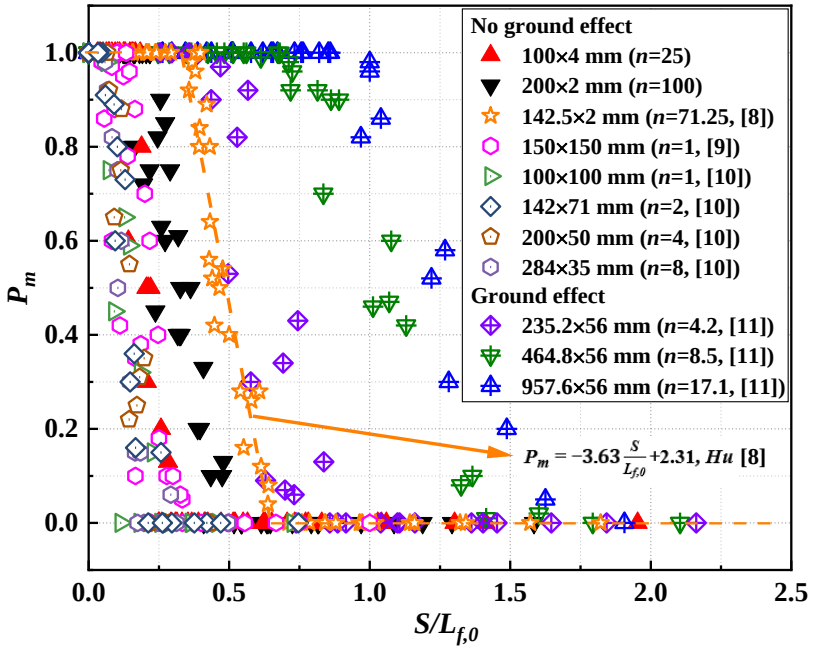

Fig. 6. P_m with different *n* against $\frac{S}{L_{f,0}}$

The dimensionless HRR of a single linear flame was defined as [27, 32].

$$\dot{Q}^* = \frac{\dot{Q}}{\rho_\infty c_p T_\infty \sqrt{g} L W^{\frac{3}{2}}} \tag{8}$$

Writing *n* explicitly in Eq. (8), the $\dot{Q}^*$ involving $\dot{Q}$, *n*, *L* and *W* is rewritten as

$$\dot{Q}^* = \frac{n\dot{Q}}{\rho_\infty c_p T_\infty \sqrt{g} L^2 W^{\frac{1}{2}}} \tag{9}$$

where ρ_∞, c_p, T_∞, g are the density and specific heat of air, ambient temperature, and gravitational acceleration. According to Eq. (7), P_m can be correlated with $\dot{Q}^*$ and the dimensionless burner spacing $\frac{S}{L_{f,0}}$ simultaneously, which gives

$$P_m = f\left(\dot{Q}^*, \frac{S}{L_{f,0}}\right) \tag{10}$$

Previous studies have shown that the entrainment characteristics of a buoyancy-controlled linear flame is related to the 2/3 power of $\dot{Q}^*$ [32, 33]. Based on this, we try to deduce the correlation of P_m and $\dot{Q}^{*\frac{2}{3}}$ by introducing a new function, $C + \frac{\mathbf{1}}{\dot{\boldsymbol{Q}}^{*\frac{\mathbf{2}}{\mathbf{3}}}}$, to Hu's model [9] as

$$P_m = A\frac{S}{L_{f,0}}\left(C + \frac{\mathbf{1}}{\dot{\boldsymbol{Q}}^{*\frac{\mathbf{2}}{\mathbf{3}}}}\right) + B \tag{11}$$

It should be noted that Eq. (11) is focused on the intermittently merging (regime II). For the aspect ratio ranging in 1-100, the range of $\dot{Q}^{*\frac{2}{3}}$ is calculated to be 1-114 for the current experiments. Since the range of $\dot{Q}^*$ is fairly large, the impact of $\frac{1}{\dot{Q}^{*\frac{2}{3}}}$ on the merging probability is strong, which significantly weakens the influence of S when its value is approaching 0. In a dual linear flames system, the air entrainment restriction decreases significantly as approaching the flame tip. Therefore, when $\dot{Q}^*$ increases to a certain level, the air entrainment restriction no longer increases notably with increasing $\dot{Q}^*$, as the flame becomes relatively thin. Under such circumstance, the air entrainment restriction reaches its limit. So, it is need to introduce a constant C to denote the limit of air entrainment restriction, and also maintain the values of $\frac{S}{L_{f,0}}$ and $C + \frac{\mathbf{1}}{\dot{\boldsymbol{Q}}^{*\frac{\mathbf{2}}{\mathbf{3}}}}$ at the same order of magnitude so as to balance the influences of S and $\dot{Q}^*$ on the merging probability.

The revised model is fitted to the experimental and literature data to determine the constant, C, and the result is shown in Fig. 7. It is found that when C equals to 0.2, the model gives the best fit to the data, while A and B is respective -9.45 and 1.48. Moreover, according to the flame merging behaviors, the merging probability in Fig. 7 is divided into three regimes [28]. As a result, a piecewise model is developed for the merging probability of two linear diffusion flames with different aspect ratios as

$$P_m = \begin{cases} 1, & \text{Regmine I: } \frac{S}{L_{f,0}}\left(0.2 + \frac{1}{\dot{Q}^{*\frac{2}{3}}}\right) < 0.05 \\ -9.45\frac{S}{L_{f,0}}\left(0.2 + \frac{1}{\dot{Q}^{*\frac{2}{3}}}\right) + 1.48, & \text{Regmine II: } 0.05 \le \frac{S}{L_{f,0}}\left(0.2 + \frac{1}{\dot{Q}^{*\frac{2}{3}}}\right) \le 0.16 \\ 0, & \text{Regmine III: } \frac{S}{L_{f,0}}\left(0.2 + \frac{1}{\dot{Q}^{*\frac{2}{3}}}\right) > 0.16 \end{cases} \tag{12}$$

In the model, Regime I denotes the "completely merging" state of which the merging probability maintains as 1 and $\frac{S}{L_{f,0}}\left(0.2+\frac{1}{\dot{Q}^{*\frac{2}{3}}}\right)$ is less than 0.05. Regime II belongs to the "intermittently merging" state of which the merging probability can be determined using the revised model with a $\frac{S}{L_{f,0}}\left(0.2+\frac{1}{\dot{Q}^{*\frac{2}{3}}}\right)$ between 0.05 and 0.16, while the flames in Regime III do not merge therefore the merging probability equals to 0 and the $\frac{S}{L_{f,0}}\left(0.2+\frac{1}{\dot{Q}^{*\frac{2}{3}}}\right)$ is over 0.16.

As shown in Fig. 6, Liu et al. [13] carried out a set of flame merging experiments with a ground flushed at the same level with the burner outlet. When the ground is existing, the air cannot flow through the bottoms and gap of burners, thus, the entrainment is more restricted compared to the cases without ground effect. From Fig. 6, it is clearly seen that the merging probability increases significantly with ground effect. As analyzed above, the air entrainment restricted by the two burners is mainly affected by the aspect ratio, which determines the flow path at the burner bottoms, as shown in Fig. 7. Therefore, the degree of air entrainment restriction caused by the ground can be directly related to *n*. Based on this presumption, the $\dot{Q}^*$ is modified by increasing the power index of *n* to obtain a new dimensionless HRR, $\dot{Q}_n^*$. It is found that a power index of 5/2 increased from 1 gives the best fit to the literature data. Therefore, $\dot{Q}_n^*$ can be expressed as

$$\dot{Q}_n^* = \frac{n^{\frac{5}{2}}\dot{Q}}{\rho_\infty c_p T_\infty \sqrt{g} L^2 W^{\frac{1}{2}}} \tag{13}$$

Similarly, the merging probability with ground effect is

$$P_m = f(\dot{Q}_n^*, \frac{S}{L_{f,0}}) \tag{14}$$

By introducing $C+\frac{1}{\dot{Q}_n^{*\frac{2}{3}}}$, the model result is also shown in Fig. 7. Same as the cases without ground effect, when *C* is 0.2, the model gives the best fit to the data obtained by Liu et al. [13]. The merging probability model is generalized as

$$P_m = \begin{cases} 1, & \text{Regmine I: } \frac{S}{L_{f,0}}\left(0.2+\frac{1}{\dot{Q}_n^{*\frac{2}{3}}}\right) < 0.21 \\ -5.03\frac{S}{L_{f,0}}\left(0.2+\frac{1}{\dot{Q}_n^{*\frac{2}{3}}}\right)+2.07, & \text{Regmine II: } 0.21 \le \frac{S}{L_{f,0}}\left(0.2+\frac{1}{\dot{Q}_n^{*\frac{2}{3}}}\right) \le 0.41 \\ 0, & \text{Regmine III: } \frac{S}{L_{f,0}}(0.2+\frac{1}{\dot{Q}_n^{*\frac{2}{3}}}) > 0.41 \end{cases} \tag{15}$$

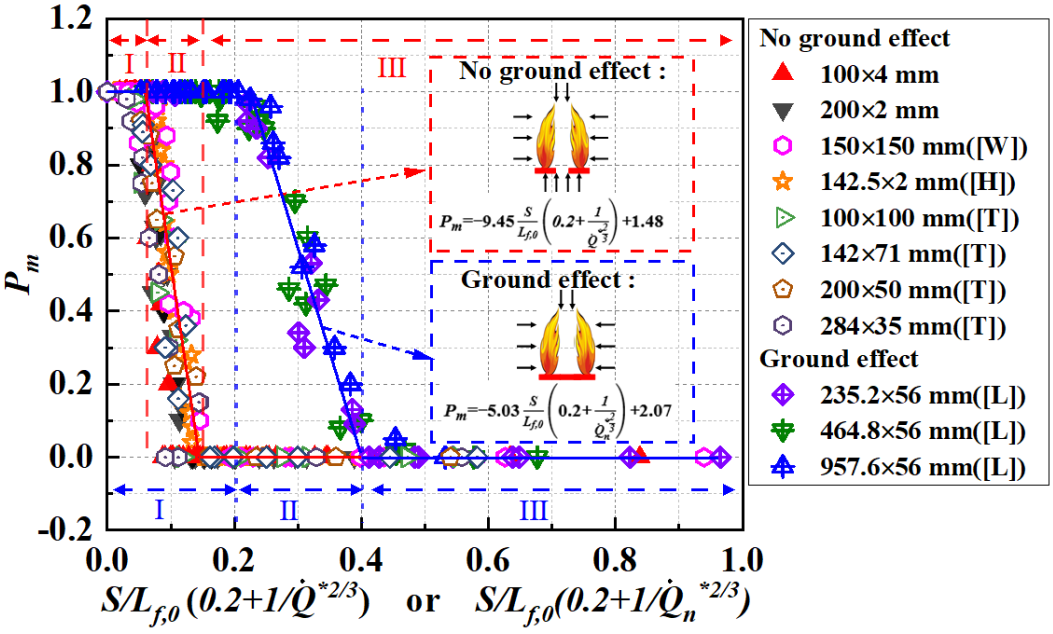

Fig. 7. Models of P_m with and without ground effects

Based on the above analysis, the current paper confirms that the merging probability is affected by the HRR, burner spacing and aspect ratio simultaneously, and the ground also has an impact on the flame merging behaviors. Therefore, the experimental conditions should be clarified across different studies [9-12] in order to reasonably compare the data for broader applications.

3.3 Merging flame height

Zukoski et al. [34] defined the height with the intermittency of 0.5 as the average flame height. For merging flame, the definition of average flame height is slightly different. In the current paper, the same definition used in most previous researches for merging flame height is applied, which is that when $P_m \geq 0.5$ the height of 0.5 appearance probability is defined as the average flame height, and when $P_m < 0.5$ the average height of the two flames is regarded as the average flame height [10].

Figure 8 shows the merging flame height varying with the burner spacing. As shown in Fig. 8, the merging flame height presents a non-monotonic trend with increasing *S*, that is, as *S* increases the merging flame height firstly drops to a local minimum and then increases to a local maximum and decreases again until becoming stable, when the dual flames are fully separated. In theory, the merging flame height is a result of the competition of two effects. On the one hand, the restriction of air entrainment induced by flame merging reduces the air supply for complete burning, leading to an increase of flame height. On the other hand, the air entrainment between two burners leads to a pressure drop in the center of two flames and thus a pressure difference at the two long sides of flame, which pushes the flame to tilt and bend, leading to a decrease of flame height.

Usually, the tilting and bending effects are overwhelmed by the enhancing effect when the flame momentum is strong enough under high HRR. However, for low HRR cases such as those in the current study, the tilting and bending become more noticeable. As seen in Fig. 4, when the merging flame height

reaches the local minimum, the flames are tilted and even bent over, leading to a notable increase in flame width. The local minimum takes place while the flames still merge, and as S increases, the restriction of air entrainment becomes weaker. Hence, the pressure difference between the two sides of both flames gradually decreases. With the decrease of tilting and bending effects, the flame height increases again. Further increasing S, the restriction of air entrainment no longer exists, and the air supply becomes sufficient for completely burning, resulting in a decrease in flame height, which is consistent with the trends in the literature [2, 10, 35-37]. When the burner spacing S is large enough, the two flames burn freely. Thus, the flame height is the same as the stand-alone flame.

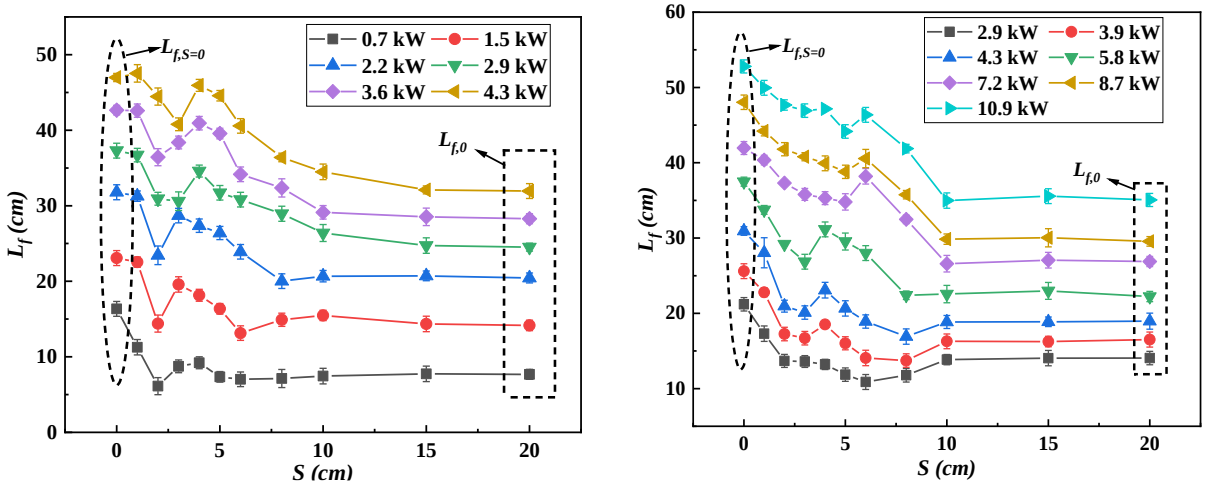

(a) 100×4 mm (b) 200×2 mm

Fig. 8. Merging flame height against S

In the previous studies, the merging flame height was usually divided by a certain characteristic length, L_c, to produce its dimensionless term. The merging flame height was found to have a positive correlation with the dimensionless HRR. The dimensionless HRR was usually written in the form of $\frac{2\dot{Q}}{\rho_\infty c_p T_\infty \sqrt{g} L_c^{\frac{5}{2}}}$ or $\frac{\dot{Q}}{\rho_\infty c_p T_\infty \sqrt{g} L_{c1} L_c^{\frac{3}{2}}}$ where L_{c1} is a dimension variable [2, 4, 38-41]. For linear flames, Hu et al. [9] believed that entrainment perimeter should have a strong effect on the merging flame height and proposed a modified entrainment perimeter, P, as the characteristic length for predicting the merging flame height, L_f, with dimensionless HRR $\dot{Q}_P^*$. The proposed model is

$$\frac{L_f}{P} = 3.68 \dot{Q}_P^{*\frac{2}{3}} \tag{16}$$

where $P = L + 2W + S + \alpha L$, $\alpha = \frac{S - 0.36 L_{f,0}}{S}$, $\dot{Q}_P^* = \frac{2\dot{Q}}{\rho_\infty c_p T_\infty \sqrt{g} P^{\frac{5}{2}}}$. Figure 9 shows the model results of $\dot{Q}_P^*$ for the experimental and literature data. It can be seen that Eq. (16) can not be applied to the experimental conditions other than Ref. [9]. Therefore, based on Hu's theory [9], this paper tries to develop a new dimensionless HRR for broader applications. From the experimental and literature data, it can be inferred that the merging flame height is closely related to the HRR, S, L and W, which is

$$L_f = f(\dot{Q},\ S,\ L,\ W) \tag{17}$$

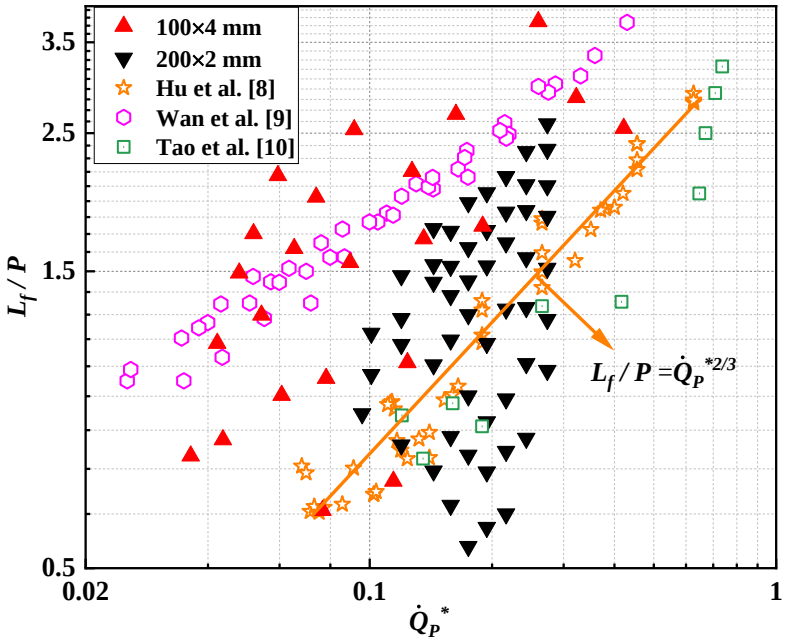

Fig. 9. $\frac{L_f}{P}$ against $\dot{Q}_P^*$

For linear diffusion flames, the flame is thin, and the flame tip is not so identifiable. Therefore, the entrainment perimeter of the flame needs to be considered. The dual flames system is symmetrical, and the entrainment process of the two flames can be regarded as basically the same. Therefore, the air entrainment perimeter of a single flame is:

$$R = L + 2W + S \tag{18}$$

In the meantime, the burner length has strong effects on the air entrainment, which should also be involved. The effective entrainment perimeter R combines the burner size and spacing, which reflects the effects of flame entrainment on the merging flame height. Then, the characteristic length in $\dot{Q}_P^*$ is replaced with R to obtain $\dot{Q}_R^*$:

$$\dot{Q}_R^* = \frac{\dot{Q}}{\rho_\infty c_p T_\infty \sqrt{g} L R^{\frac{3}{2}}} \tag{19}$$

The merging flame height can be expressed as

$$\frac{L_f}{R} = f(\dot{Q}_R^*) \tag{20}$$

The experimental data in the current study and literature are used to perform a data fitting to obtain the coefficient and power index of $\dot{Q}_R^*$ in Eq. (20). As shown in Fig. 10, with an exponential fitting, the final model of merging flame height is determined as

$$\frac{L_f}{R} = 3.92\dot{Q}_R^{*\frac{4}{5}} \tag{21}$$

which can well predict all other merging flame heights measured in the literature by Wan [10], Hu [9], and Tao [11] with different HRRs and aspect ratios.

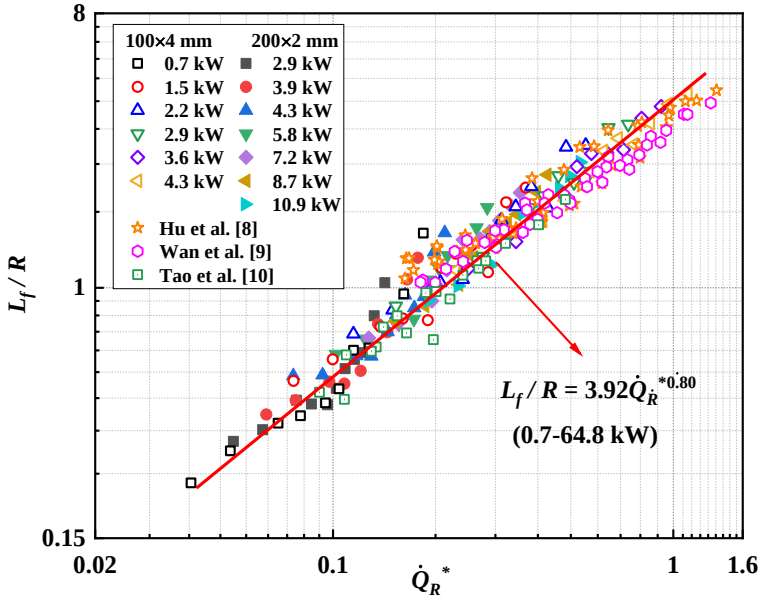

Fig. 10. $\frac{L_f}{R}$ against $\dot{Q}_R^*$

Figure 11 further shows the comparison of calculated and experimental merging flame heights. It is seen that the error of predictions is almost within the range of ±20% of experimental measurements. Therefore, the proposed model can be applied to a wider range of experimental conditions than those in the current study.

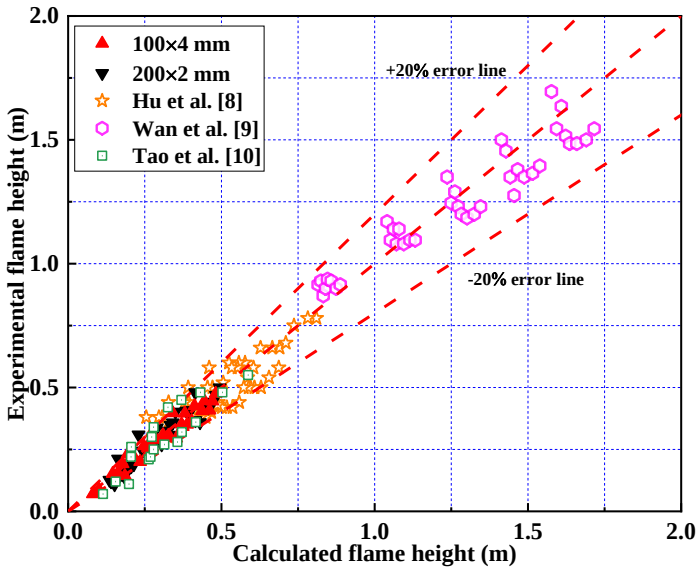

Fig. 11. Comparison of calculated and experimental merging flame heights

4 Conclusions

In this paper, the merging dynamics of dual parallel linear diffusion flames with low heat release rates and high aspect ratios are studied. The main factors affecting the merging probability and merging flame height, including HRR, burner spacing, aspect ratio, ground effect, are analyzed. The main conclusions are generalized as follows.

1. Increasing HRR enhances the entrainment rate, while increasing aspect ratio increases the area with restricted air entrainment. Both effects make the flames easier to merge. Based on this, the current paper combines the dimensionless HRR, $\dot{Q}^*$, which involves HRR and aspect ratio of burner with the dimensionless burner spacing, $\frac{S}{L_{f,0}}$, to develop a new piecewise prediction model for the merging probability. By introducing a new function of $C + \frac{\mathbf{1}}{\dot{\boldsymbol{Q}}^{*\frac{\mathbf{2}}{\mathbf{3}}}}$, it is found that when *C*=0.2, the model performs well with different HRRs and aspect ratios and $P_m \propto -\frac{1}{\dot{Q}^{*\frac{2}{3}}}$.

2. The presence of ground inhibits the air flowing through the bottom and gap between the two burners and thus enhances the restriction of air entrainment, resulting in a higher merging probability. Therefore, the $\dot{Q}^*$ is modified by increasing the power index of aspect ratio to obtain $\dot{Q}_n^*$, and $P_m \propto -\frac{1}{\dot{Q}_n^{*\frac{2}{3}}}$ is identified by fitting the experimental data. The influence of the aspect ratio on the merging probability increases from the 1st power to the 2.5th power.

3. The merging flame height shows a non-monotonic trend with increasing burner spacings. The trend is a result of the competition of enhanced flame height led by merging and tilting and bending effects caused by the pressure difference. Analyzing the air entrainment mechanism of dual merging flames, the effective entrainment perimeter of a single burner, R, is introduced as the characteristic length to develop the dimensionless HRR, $\dot{Q}_R^*$. By fitting the experimental data in the current study and literature, it is found that the merging flame height and $\dot{Q}_R^*$ has a positive correlation of $\frac{L_f}{R} = 3.92\dot{Q}_R^{*\frac{4}{5}}$. The proposed model is suitable for a wider range of experimental conditions than those in the current study.

CRediT authorship contribution statement

Kaiyuan Li: Supervision, Writing – review & editing, Funding acquisition. **Zhuangzhuang Ma**: Writing – original draft, Formal analysis. **Xinyan Huang**: Writing – review & editing, Conceptualization. **Yanyan Zou**: Data curation.

Acknowledgments

This work was supported by National Natural Science Foundation of China (NSFC) under Grant No. 51876148.

Appendix A. Supplementary data

Supplementary data to this article can be found online at https://doi.org/10.1016/j.firesaf.2021.103490.

References

[1] Liu Y, Liu H, Zhou Y, Sun C. Spread vector induced cellular automata model for real-time crown fire behavior simulation. Environ Model Software 2018;108:14-39.https://doi.org/10.1016/j.envsoft.2018.07.005.

[2] Ji J, Wan H, Gao Z, Fu Y, Sun J, Zhang Y, et al. Experimental study on flame merging behaviors from two pool fires along the longitudinal centerline of model tunnel with natural ventilation. Combust Flame 2016;173:307-18.https://doi.org/10.1016/j.combustflame.2016.08.020.

[3] Wan H, Gao Z, Ji J, Li K, Sun J, Zhang Y. Experimental study on ceiling gas temperature and flame performances of two buoyancy-controlled propane burners located in a tunnel. ApEn 2017;185:573-81.https://doi.org/10.1016/j.apenergy.2016.10.131.

[4] Wang Q, Wang S, Liu H, Shen J, Shang F, Shi C, et al. Characterization of ceiling smoke temperature profile and maximum temperature rise induced by double fires in a natural ventilation tunnel. Tunnel Underground Space Technol 2020;96.https://doi.org/10.1016/j.tust.2019.103233.

[5] Huang Y, Wan H, Ding L, Ji J, Wang C. Research on the interaction between two line jet fires with unequal heat release rate at different burner distances. Fuel 2019;258.https://doi.org/10.1016/j.fuel.2019.116016.

[6] Yu L, Wan H, Gao Z, Ji J. Study on flame merging behavior and air entrainment restriction of multiple fires. Energy 2020.https://doi.org/10.1016/j.energy.2020.119470.

[7] Vasanth S, Tauseef SM, Abbasi T, Abbasi SA. Multiple pool fires: Occurrence, simulation, modeling and management. J Loss Prev Process Indust 2014;29(1):103-21.https://doi.org/10.1016/j.jlp.2014.01.005.

[8] Yang T, Xia X, Zhang P. Vortex-dynamical interpretation of anti-phase and in-phase flickering of dual buoyant diffusion flames. Physical Review Fluids 2019;4(5).https://doi.org/10.1103/PhysRevFluids.4.053202.

[9] Hu L, Huang L, Wang Q, Kuwana K. Experimental study and analysis on the interaction between two slot-burner buoyant turbulent diffusion flames at various burner pitches. Combust Flame 2017;186:105-13.https://doi.org/10.1016/j.combustflame.2017.07.033.

[10] Wan H, Ji J, Li K, Huang X, Sun J, Zhang Y. Effect of air entrainment on the height of buoyant turbulent diffusion flames for two fires in open space. Proceedings of the Combustion Institute 2017;36(2):3003-10.https://doi.org/10.1016/j.proci.2016.07.078.

[11] Tao C, Ye Q, Wei J, Shi Q, Tang F. Experimental Study on Flame–Flame Interaction and Its Merging Features Induced by Double Rectangular Propane Diffusion Burners With Various Aspect Ratios. Combust Sci Technol 2018;191(8):1416-29.https://doi.org/10.1080/00102202.2018.1529031.

[12] Liu N, Zhang S, Luo X, Lei J, Chen H, Xie X, et al. Interaction of two parallel rectangular fires. Proceedings of the Combustion Institute 2019;37(3):3833-41.https://doi.org/10.1016/j.proci.2018.06.158.

[13] Bunkwang A, Matsuoka T, Nakamura Y. Mode transition of interacting buoyant non-premixed flames. Journal of Thermal Science and Technology 2020;15(1):JTST0003-JTST.https://doi.org/10.1299/jtst.2020jtst0003.

[14] Sugawa O, Takahashi W. Flame height behavior from multi‐fire sources. Fire Mater 1993;17(3):111-7.https://doi.org/10.1002/fam.810170303.
[15] Kamikawa D, Weng WG, Kagiya K, Fukuda Y, Mase R, Hasemi Y. Experimental study of merged flames from multifire sources in propane and wood crib burners. Combust Flame 2005;142(1-2):17-23.https://doi.org/10.1016/j.combustflame.2005.02.004.
[16] Delichatsios MA. A Correlation for the Flame Height in " Group " Fires. fire science and technology 2007;26(1):1-8.https://doi.org/10.3210/fst.26.1.
[17] Wang K, Tao C, Liu Q, Qian Y, He P. An experimental investigation of flame height and air entrainment rate of double jet fires. ExHT 2017;31(1):22-31.https://doi.org/10.1080/08916152.2017.1339140.
[18] Liu C, Liu X, Ge H, Deng J, Zhou S, Wang X, et al. On the influence of distance between two jets on flickering diffusion flames. Combust Flame 2019;201:23-30.https://doi.org/10.1016/j.combustflame.2018.12.003.
[19] He P, Wang P, Wang K, Liu X, Wang C, Tao C, et al. The evolution of flame height and air flow for double rectangular pool fires. Fuel 2019;237:486-93.https://doi.org/10.1016/j.fuel.2018.10.027.
[20] Wan H, Gao Z, Ji J, Fang J, Zhang Y. Experimental study on horizontal gas temperature distribution of two propane diffusion flames impinging on an unconfined ceiling. International Journal of Thermal Sciences 2019;136:1-8.https://doi.org/10.1016/j.ijthermalsci.2018.10.010.
[21] Li B, Wan H, Gao Z, Ji J. Experimental study on the characteristics of flame merging and tilt angle from twin propane burners under cross wind. Energy 2019;174:1200-9.https://doi.org/10.1016/j.energy.2019.03.061.
[22] Wan H, Gao Z, Ji J, Zhang Y. Experimental study on flame radiant heat flux from two heptane storage pools and its application to estimating safety distance. Energy 2019;182:11-20.https://doi.org/10.1016/j.energy.2019.06.006.
[23] Thomas PH, Baldwin R, Heselden AJM. Buoyant diffusion flames: Some measurements of air entrainment, heat transfer, and flame merging. Symposium (International) on Combustion 1965;10(1):983-96.https://doi.org/10.1016/S0082-0784(65)80241-7.
[24] Cetegen BM, Ahmed TA. Experiments on the periodic instability of buoyant plumes and pool fires. Combust Flame 1993;93(1):157-84.https://doi.org/10.1016/0010-2180(93)90090-P.
[25] Xie G, Wen L. Image Edge Detection Based On Opencv. International Journal of Electronics and Electrical Engineering 2013;1(2):104-6.https://doi.org/10.12720/ijeee.1.2.104-106.
[26] Otsu N. A threshold selection method from gray-level histograms. IEEE Trans Syst Man Cybern 1979;26(8):62.https://doi.org/10.1109/TSMC.1979.4310076.
[27] Zhang X, Hu L, Zhang X, Yang L, Wang S. Non-dimensional correlations on flame height and axial temperature profile of a buoyant turbulent line-source jet fire plume. J Fire Sci 2014;32(5):406-16.https://doi.org/10.1177/0734904114529258.
[28] Lu K, Hu L, Delichatsios M, Tang F, Qiu Z, He L. Merging behavior of facade flames ejected from two windows of an under-ventilated compartment fire. Proceedings of the Combustion Institute 2015;35(3):2615-22.https://doi.org/10.1016/j.proci.2014.05.083.
[29] Delichatsios MA. Transition from momentum to buoyancy-controlled turbulent jet diffusion flames and flame height relationships. Combust Flame 1993;92(4):349-64.https://doi.org/10.1016/0010-2180(93)90148-V.
[30] Wang Z, Gao Z. A new flux prediction model for laminar and turbulent flow regimes in constant pressure cross-flow microfiltration. Journal of Environmental Chemical Engineering

2021.https://doi.org/10.1016/j.jece.2021.106156.
[31] Zhou K, Zhang L, Huang M, Zhou M, Wang C. Experimental study on flame interaction and geometrical features of two identical fires on a slope. Fire Saf J 2021;126.https://doi.org/10.1016/j.firesaf.2021.103463.
[32] Yuan LM, Cox G. An experimental study of some line fires. Fire Saf J 1996;27(2):123-39.https://doi.org/10.1016/S0379-7112(96)00047-1.
[33] Karlsson B, Quintiere JG. Enclosure Fire Dynamics. CRC Press 2000
[34] Zukoski EE, Cetegen BM, Kubota T. Visible structure of buoyant diffusion flames. Symposium (International) on Combustion 1985;20(1):361-6.https://doi.org/10.1016/S0082-0784(85)80522-1.
[35] Hu L, Liu S, Zhang X. Flame heights of line-source buoyant turbulent non-premixed jets with air entrainment constraint by two parallel side walls. Fuel 2017;200:583-9.https://doi.org/10.1016/j.fuel.2017.03.082.
[36] Wan H, Gao Z, Ji J, Wang L, Zhang Y. Experimental study on merging behaviors of two identical buoyant diffusion flames under an unconfined ceiling with varying heights. Proceedings of the Combustion Institute 2019;37(3):3899-907.https://doi.org/10.1016/j.proci.2018.05.154.
[37] Wan H, Gao Z, Ji J, Zhang Y, Li K, Wang L. Effects of pool size and spacing on burning rate and flame height of two square heptane pool fires. J Hazard Mater 2019;369:116-24.https://doi.org/10.1016/j.jhazmat.2019.01.111.
[38] Gao Z, Ji J, Wan H, Li K, Sun J. An investigation of the detailed flame shape and flame length under the ceiling of a channel. Proceedings of the Combustion Institute 2015;35(3):2657-64.https://doi.org/10.1016/j.proci.2014.06.078.
[39] Fan CG, Tang F. Flame interaction and burning characteristics of abreast liquid fuel fires with cross wind. Exp Therm Fluid Sci 2017;82:160-5.https://doi.org/10.1016/j.expthermflusci.2016.11.010.
[40] Hu L, Zhang X, Delichatsios MA, Wu L, Kuang C. Pool fire flame base drag behavior with cross flow in a sub-atmospheric pressure. Proceedings of the Combustion Institute 2017;36(2):3105-12.https://doi.org/10.1016/j.proci.2016.06.139.
[41] Zhang S, Liu N, Lei J, Xie X, Jiao Y, Tu R. Experimental study on flame characteristics of propane fire array. International Journal of Thermal Sciences 2018;129:171-80.https://doi.org/10.1016/j.ijthermalsci.2018.02.024.